Cleaner Engineering and Technology 31 (2026) 101173

Contents lists available at ScienceDirect

Cleaner Engineering and Technology

journal homepage: www.sciencedirect.com/journal/cleaner-engineering-and-technology

Towards a performance map of gyroid structures for varying cell size: Trade-off between carbon footprint and structural performance

Giulia Colombini *, Silvio Defanti, Federico Torri, Elena Bassoli

Department of Engineering "Enzo Ferrari" (DIEF), University of Modena and Reggio Emilia, Via P. Vivarelli, 10, 41125, Modena, MO, Italy

A R T I C L E I N F O

Keywords:
Laser powder bed fusion
TPMS structures
Life cycle assessment
Productivity
Global warming potential

A B S T R A C T

Additive manufacturing (AM) has emerged as a transformative technology enabling the production of complex geometries that reduce component mass and improve performance, particularly through the integration of lattice structures. These lightweight architectures, characterised by a high surface-to-volume ratio, are increasingly being analysed and integrated into various technical applications due to their exclusive properties. Among the most promising configurations are Triply Periodic Minimal Surfaces (TPMS), especially gyroid structures, which offer structural and functional advantages. This study builds on new performance metrics for lattice structures that combine productivity and sustainability, addressing the growing need to prioritise carbon footprint considerations in engineering design. The research also critiques existing environmental assessment methods for their inability to fully capture the unique capabilities of advanced AM technologies. The influence of cell size variation in gyroid lattice structures fabricated via Laser Powder Bed Fusion of AlSi10Mg is evaluated on both environmental impact and productivity. The study includes four cubic specimens with cell dimensions varying from 4 to 12 mm but consistent wall thickness and performs a comparative cradle-to-gate life cycle assessment to evaluate the environmental impact, particularly in terms of carbon emissions. The results quantify the improvement in structural performance and the simultaneous increase in manufacturing time and resource consumption as cell size decreases, leading to the conclusion that the carbon footprint per unit strength or stiffness of the 6 mm cell is 2 to 3 times lower than that of the 12 mm cell. The trade-off between the conflicting requirements is presented in a performance map that serves as a decision-making tool in the current landscape where carbon footprint is being incorporated into product specifications alongside technical requirements.

1. Introduction

The emergence and development of Additive Manufacturing (AM) have enabled the production of complex shapes previously unattainable with traditional manufacturing methods, leading to a paradigm shift in geometric design for enhanced component performance. Among these innovations, lattice structures have naturally arisen, offering spatially arranged architectures with high surface-to-volume ratios that can be incorporated into topology-optimised designs. Campo et al. (2019) and Mantovani et al. (2022) used an engine mounting bracket and a steering column support, respectively, to demonstrate that tailoring lattice density allows precise control of the stiffness–mass relationship in automotive components, producing significantly lighter parts while maintaining mechanical performance comparable to solid designs.

Among lattice designs, Triply Periodic Minimal Surfaces (TPMS), and gyroid structures in particular, have attracted significant engineering interest due to their distinctive continuous, non-self-intersecting surfaces with zero mean curvature, featuring smooth, organic geometries that avoid the sharp edges and junctions typical of other lattices. These properties make TPMS particularly suitable for addressing both structural and functional requirements, while also offering opportunities to enhance material efficiency. The comprehensive review by Feng et al. (2022) highlighted that TPMS outperform conventional lattice geometries in terms of mechanical efficiency and design flexibility. Torri et al. (2023) demonstrated their superior thermal performance in heat-exchange applications compared to conventional turbulator solutions, while Verma et al. (2022) showed that TPMS-based porous scaffolds provide tunable porosity and mechanical properties, effectively meeting load-bearing requirements in biomedical applications. These studies collectively illustrate how TPMS, and gyroid structures in

* Corresponding author.
E-mail addresses: giulia.colombini@unimore.it (G. Colombini), silvio.defanti@unimore.it (S. Defanti), federico.torri@unimore.it (F. Torri), elena.bassoli@unimore.it (E. Bassoli).

https://doi.org/10.1016/j.clet.2026.101173
Received 1 September 2025; Received in revised form 22 December 2025; Accepted 15 February 2026
Available online 17 February 2026
2666-7908/© 2026 Published by Elsevier Ltd. This is an open access article under the CC BY-NC-ND license (http://creativecommons.org/licenses/by-nc-nd/4.0/).

particular, can be tailored for specific functional objectives while distinguishing themselves from beam-based lattices.

Adjusting geometrical properties of gyroid unit cells, primarily cell size and wall thickness, directly influences overall lattice structure performance. Consequently, this factor, alongside structure dimensions, requires essential consideration during design Defanti et al. (2024) investigated AlSi10Mg gyroid structures produced via Laser Powder Bed Fusion (PBF-LB/M), focusing on three unit cell sizes (6 mm, 8 mm, and 12 mm) with a constant wall thickness of 0.5 mm, limited by the technological constraints of the specific machine-parameter set-up. To accurately evaluate structural properties, samples were fabricated entirely from a gyroid geometry, with dimensions selected to preserve a consistent number of cell repetitions across all samples. Compression tests revealed that smaller unit cells enhance specific compressive strength and normalized specific plateau stress. Similarly, Yang et al. (2019) quantified, both numerically and experimentally, how variations in relative density affect stiffness and strength in PBF-LB/M Ti-6Al-4V gyroid lattices. These findings indicate that these structures can be used for precise tailoring of the structural response.

Functional performance studies further illustrate the effect of gyroid cell size. Samson et al. (2023) assessed heat-sink applications, Torri et al. (2025) evaluated automotive engine oil coolers under laminar and turbulent flow, and Mahmoud et al. (2023) investigated air-to-air heat exchangers, all considering different unit cell sizes. All three studies demonstrated that gyroid geometries enhance heat transfer compared to the reference design, due to their high surface-to-volume ratio, particularly for smaller cells. However, they also increase local pressure drop, highlighting the trade-off between efficiency and geometric design.

Beyond mechanical and thermal performance, sustainability has become a central concern for the industrial sector, driven by environmental constraints such as limited resources, regulatory pressures, and strategic competitiveness. Life Cycle Assessment (LCA) provides a robust framework to quantify the environmental impacts of manufacturing processes and design choices. Su et al. (2024) demonstrated that PBF-LB/M can offer environmental benefits when design freedom is leveraged to produce geometries that minimise material use and energy consumption. Lattice structures, particularly gyroid TPMS, represent a lightweight solution that contributes to next-generation eco-materials: Sikandar et al. (2023) showed that integrating lattices into lever arms can significantly reduce CO_2 emissions compared to solid components, primarily through material savings. However, the environmental footprint of PBF-LB/M is strongly influenced by build time and energy consumption, which increase for intricate geometries, as highlighted by Colombini et al. (2024). Despite the growing adoption of gyroid structures for their mechanical and thermal advantages, systematic studies are still lacking on how geometric parameters simultaneously affect performance, productivity, and environmental impact.

This study aims to evaluate the productivity and environmental impact of gyroid structures fabricated using PBF-LB/M. Specifically, it examines how these outcomes vary with the characteristic unit cell size, providing a framework for introducing new metrics to map the performance of these structures across structural, environmental, and economic dimensions within a cradle-to-gate LCA system boundary. This approach offers quantitative insights to support design decisions in various application scenarios.

2. Materials and methods

2.1. Goal and scope definition

The aim of the LCA is to provide a thorough quantitative analysis of the environmental impacts associated with the manufacture of gyroid structures using the PBF-LB/M process. This assessment is carried out using a cradle-to-gate approach covering the main stages of the life cycle such as raw material production (extraction and gas atomisation for powder production) and fabrication of the parts. Downstream activities, such as material handling and post-processing, are excluded as they would be identical for all specimens and therefore would not influence the comparative analysis of environmental impacts across cell sizes. This study adopts a methodological framework inspired by Colombini et al. (2025), which examined the sustainability dimensions of the same technological system applied for the production of such complex architectures. To achieve the goals of this analysis, a specific cubic geometry of 48 mm side, consisting entirely of the gyroid lattice structure is chosen as the functional unit without skin or additional bulk parts. Therefore, four cube-shaped samples (Fig. 1) with different unit cell sizes (12, 8, 6, and 4 mm) are designed, with the wall thickness set to 0.5 mm in accordance with the results of Sola et al. (2020). In that study, the technological feasibility of lattice materials fabricated using the same technique is assessed, demonstrating that very thin features approach the limits of process capabilities and the minimum detail sizes must be constrained relative to the melt pool dimensions to avoid defective fabrication. The dimensions of the samples are set to a uniform length of 48 mm per side to ensure an integer number of unit cells within the given volume.

The main nominal features of the individual samples are summarised in Table 1. The nominal relative density, defined as the ratio of the lattice density to that of the solid bulk material, is also given in the table. It shows that the relative density ranges between 11% and 31% with decreasing unit cell size, which illustrates the significant influence of cell size on the properties of the meta-material that can be used in specific applications.

The MathMod-10 software is used to generate the geometry of a fundamental gyroid patch, which is then meshed and mirrored with Altair® HyperMesh to create the unit cell. The elementary shape is then replicated in three dimensions to create the final sample geometries, which are then converted to STL format. This workflow is consistent with the approach reported by Defanti et al. (2024), who used parametric TPMS modelling to generate geometries for the experimental evaluation of mechanical behaviour. The triangular representation in STL files, combined with the complexity of curved geometries, leads to large file sizes, particularly for smaller cells with proportionally larger surface areas. As discussed in the critical analysis by Azman et al. (2018) regarding the inadequacy of current CAD file formats for designing lattice structures, large files present a challenge for handling and management, especially in subsequent industrial processing. To address this issue, the number of triangles is reduced using Materialise Magics 25 software (Materialise Software, Leuven, Belgium). In this step, a maximum geometric deviation of 0.025 mm, an angle limit of 4° and 10 iterations are applied. The shape approximation obtained with this protocol is expected to be overridden by the resolution of the PBF-LB/M process. This approach reduces file size, thereby streamlining data handling and processing.

Each sample is consolidated with a layer thickness of 50 μm using the aluminium alloy AlSi10Mg. Manufacturing is carried out on an SLM 280 dual laser machine (NIKON SLM Solutions GmbH, Lübeck, Germany). For the purpose of this analysis, each sample is assumed to be manufactured in a dedicated job, with a positioning on the build platform that allows consolidation with only one of the two lasers. Due to the self-supporting nature of the gyroid structures, no additional support structures are required during fabrication. A contour-core scanning strategy is applied for all the four parts, with the internal regions processed using a laser power of 350 W, a scanning speed of 1150 mm/s, and a hatch distance of 0.17 mm, while the outer contour is consolidated with 300 W laser power and a slower scanning speed of 600 mm/s to enhance surface quality. In general, scanning strategies that are tailored to thin-walled structures and ensure a higher standard of accuracy and surface quality are favoured for this type of complex geometries, as demonstrated in the investigation by Defanti et al. (2024). In this case, as reported in Fig. 2, most of the scanned areas within each layer are contour regions, with the core areas limited to smaller portions of the geometry, such as the "saddle" areas. Therefore, the chosen strategy

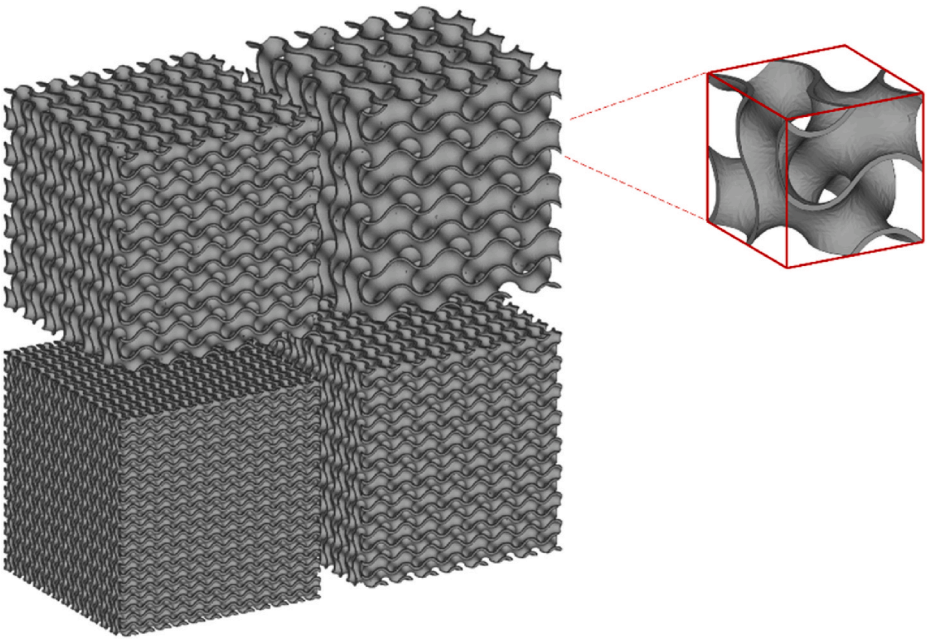

Fig. 1. Functional unit of the four cell sizes analysed and example of a unit cell (in the red box).

Table 1
Geometric configuration and estimated mass of the samples.

Part ID	Unit cell dimension [mm]	Cell count [X × Y × Z]	Volume [cm^3]	Surface area [cm^2]	Nominal relative density (ρ rel %)	Estimated mass [g]
G-size 4	4	4 × 4 × 4	34.7	3.9	31%	93.3
G-size 6	6	6 × 6 × 6	25.4	2.5	23%	68.3
G-size 8	8	8 × 8 × 8	19.0	1.9	17%	51.2
G-size 12	12	12x12x12	12.1	1.2	11%	32.5

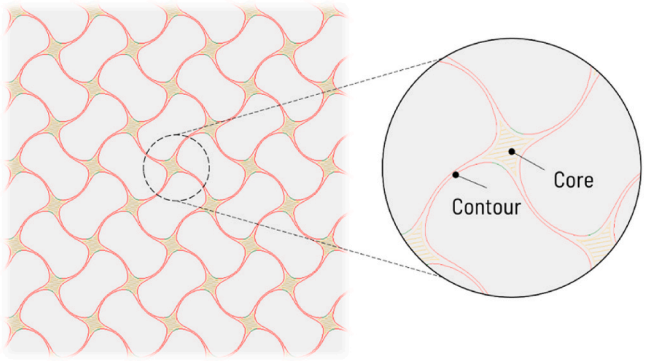

Fig. 2. Scanning strategy, showing the laser paths on a slice of the gyroid structure.

should ensure an effective balance between productivity and accuracy without compromising the feasibility of the part. For this case study, the recoating system is set to a speed of 400 rpm, which corresponds to a time of 12 s to spread a layer of metal powder, with a minimum scan time of zero seconds.

2.2. Process modelling and inventory development

After establishing the manufacturing conditions and defining the scope and boundaries of the analysis, a structured data strategy is developed to systematically identify and gather the input resources needed for the Life Cycle Inventory (LCI). The investigation followed the Unit Manufacturing Process (UMP) approach in combination with the Process Life Cycle Inventory framework, evaluating therefore each manufacturing operation as a transformation unit that converts specific inputs into output quantities. This modeling philosophy is formalized in ASTM E2986–22, and ASTM E2986–22 standards, which define and provide guidance on applying UMP-based inventories to quantify resource and emission flows across manufacturing systems. Consistently with these standards, Ramirez-Cedillo et al. (2021) demonstrated the practical implementation of the UMP and Process LCI framework for AM processes, showing that decomposing production into discrete transformation units improves the transparency and accuracy of life cycle inventories. Therefore, a UMP representation of the technique under investigation is defined (Fig. 3), which allows the identification of the three main inputs and outputs.

Primary data for these inputs are sourced from direct experimental measurements conducted in Colombini et al. (2024) study, where a detailed life cycle inventory was performed for the same machine, material and process parameters, systematically measuring all the main resources consumption at the level of each individual machine sub-systems. Critical data points-such as metal powder consumption, the percentage of material recycling, the exact duration and energy consumption during the individual manufacturing steps and sub-systems directly incorporated into the current study, with adjustments made to reflect the specific geometry under evaluation. In addition, the manufacturing time, a crucial factor in determining the electrical energy consumption, is calculated using the machine post-processing software, based on the scanning strategy and the recoating parameters chosen during the design phase. Inventory data on powder production are taken from the literature and adapted to the current case study based on the work of Sciancalepore et al. (2017), who quantified the energy demand and environmental burdens associated with atomized metal powder production, providing suitable process-level data for the LCI.

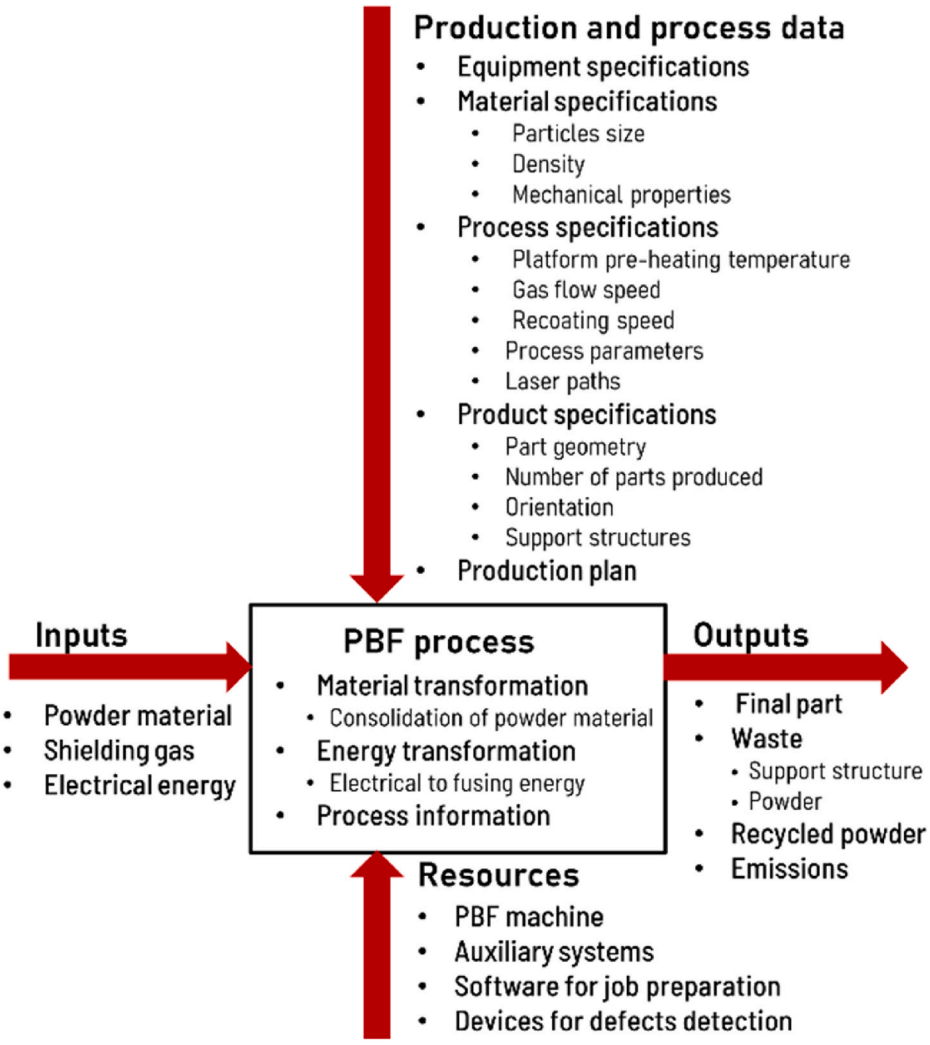

Fig. 3. Representation of the UMP for the PBF-L/M process.

To enhance the robustness, resource consumption is incorporated into the inventory model alongside supplementary datasets. Emissions of metal powder and argon, not retained by the system, are estimated using published data on capture efficiencies, enabling a more precise evaluation of their implications for human toxicity and ecological degradation. Electrical energy demand is modeled using the standard Italian grid mix, without taking into account the specific energy mix of the production site. Transport impacts are included: for feedstock, it is modeled over a distance of 1500 km, while other activities over 100 km, all using EURO6-compliant heavy-duty vehicles (16–32 tonnes).

The system and inventory data are modeled using SimaPro 9.3.0.2 software and the Ecoinvent database (version 3.8), applying an attributional approach via the Allocation at the Point of Substitution (APOS) system model. The LCA is carried out following the guidelines of the ISO 14040–14044 standards. The impact assessment is performed using the ReCiPe 2016 method, which was recognised already by Huijbregts et al. (2017) for its robustness and comprehensive coverage of environmental categories. Specifically, the evaluation is conducted at both the midpoint and endpoint levels, employing the hierarchical perspective with average weighting factors to reflect a balanced societal viewpoint on environmental priorities.

3. Results and discussion

3.1. Life cycle data inventory analysis

The time estimation analysis is presented in Table 2 and comprehends both the evaluation of the primary processing phase, referred to as construction time, which includes only laser consolidation and recoating, and the total job duration. The latter additionally takes in the constant time for the pre-processing phase, in which the build chamber and powder preparation take place, with a total time interval of 1 h and 21 min, as well as the post-processing procedures such as part cooling and chamber cleaning, which amount to 3 h and 30 min.

Using the G-size12 specimen as a reference, as it has the largest unit cell and the lowest relative density, a clear trend can be seen: reducing the cell size results in a notable increase in build time. Specifically, decreasing from 12 mm to 4 mm increases the total construction time by 11%, 22% and 42% respectively. This is mainly due to how the chosen printing strategy is applied to the gyroid structure. Although the equal number of layers, smaller cell sizes lead to greater material volume requiring consolidation, with also a higher percentage of material processed using the slower, contour-based scan strategy. In addition, most of the core areas that benefit from fast, efficient scanning strategies are represented by the saddle areas, which become smaller and more numerous as the cell size decreases. The shift towards more contour-dominated geometries, as illustrated in Fig. 4, leads to a significant

Table 2
Time segmentation required for the PBF-LB/M fabrication.

Part ID	Construction time [hh:mm]	Setup [hh:mm]	Set-off [hh:mm]	Total job duration [hh:mm]	Time increase factor
G-size 4	04:41	01:21	03:30	09:33	x4.2
G-size 6	04:03	01:21	03:30	08:54	x2.2
G-size 8	03:41	01:21	03:30	08:32	x1.1
G-size 12	03:19	01:21	03:30	08:10	Reference

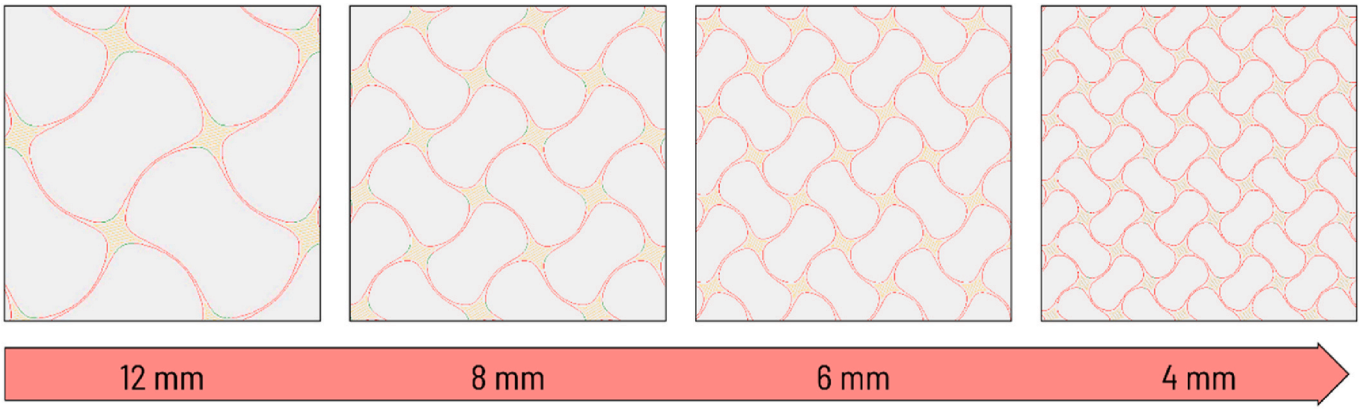

Fig. 4. Change in the laser path with the reduction in cell size.

increase in build time.

In order to quantify the electrical energy demand during the primary manufacturing phase, the job duration is integrated with empirically measured power consumption values. The energy usage during the melting stage and that of auxiliary systems (i.e. platform heating, laser cooling and argon recirculation) is directly influenced by the part geometry and thus by the production time, while the preparatory and final phases of the job and thus their respective energy consumption remain constant regardless of the structure being produced. Therefore, the geometry-related variation in production time affects the total energy consumption during the primary construction phase. A detailed breakdown of the electrical energy consumption based on these experimental measurements can be found in Table 3.

To gain a deeper insight into the distribution of power consumption in a PBF-L/M system and during a typical job, a Pareto analysis is performed, as shown in Fig. 5. The graph in Fig. 5a) relates the average power consumption (kW) for each specific sub-system, to its cumulative percentage contribution to the total consumption, represented by the grey line with square markers. The hoover, the sieving unit and the chiller are supplied with power separately from the machine, hence their consumption can be measured independently. In contrast, the supply of the other sub-systems is embedded in that of the entire machine, whose idle consumption, when no system is active, amounts to a non-negligible 0.95 kW. The power values shown in Fig. 5a) are calculated by subtracting this idle consumption for all these sub-systems, so that each impact can be assessed separately. Fig. 5b) shows the Pareto chart for the energy consumption of the main phases of the process: i) the preparatory steps required before the job can be started (consisting of platform heating, purging phase and sieving); ii) the construction itself, divided into two separate bars for the melting energy and the operation of the auxiliary systems (chiller, recirculation pump, maintenance of the platform temperature) during the build time; iii) the cooling phase; and iv) the cleaning phase. Each energy bar is obtained by multiplying the power values of the individual sub-systems and the time interval

Table 3
Estimated electrical energy demand for the construction of the samples.

Part ID	Process stage		Duration [h]	Power consumption [W]	Electrical energy [kWh]
G-size 4	Pre-processing phase	Setup	1.35	1.65	2.25
	Main processing phase	Laser melting	4.68	1.23	5.76
		Auxiliary action	4.68	3.04	14.23
	Post processing phase	Part cooling	1.00	1.00	1.00
		Chamber reset	2.50	2.20	5.50
G-size 6	Pre-processing phase	Setup	1.35	1.65	2.25
	Main processing phase	Laser melting	4.05	1.23	4.98
		Auxiliary action	4.05	3.04	12.31
	Post processing phase	Part cooling	1.00	1.00	1.00
		Chamber reset	2.50	2.20	5.50
G-size 8	Pre-processing phase	Setup	1.35	1.65	2.25
	Main processing phase	Laser melting	3.68	1.23	4.53
		Auxiliary action	3.68	3.04	11.20
	Post processing phase	Part cooling	1.00	1.00	1.00
		Chamber reset	2.50	2.20	5.50
G-size 12	Pre-processing phase	Setup	1.35	1.65	2.25
	Main processing phase	Laser melting	3.32	1.23	4.08
		Auxiliary action	3.32	3.04	10.08
	Post processing phase	Part cooling	1.00	1.00	1.00
		Chamber reset	2.50	2.20	5.50

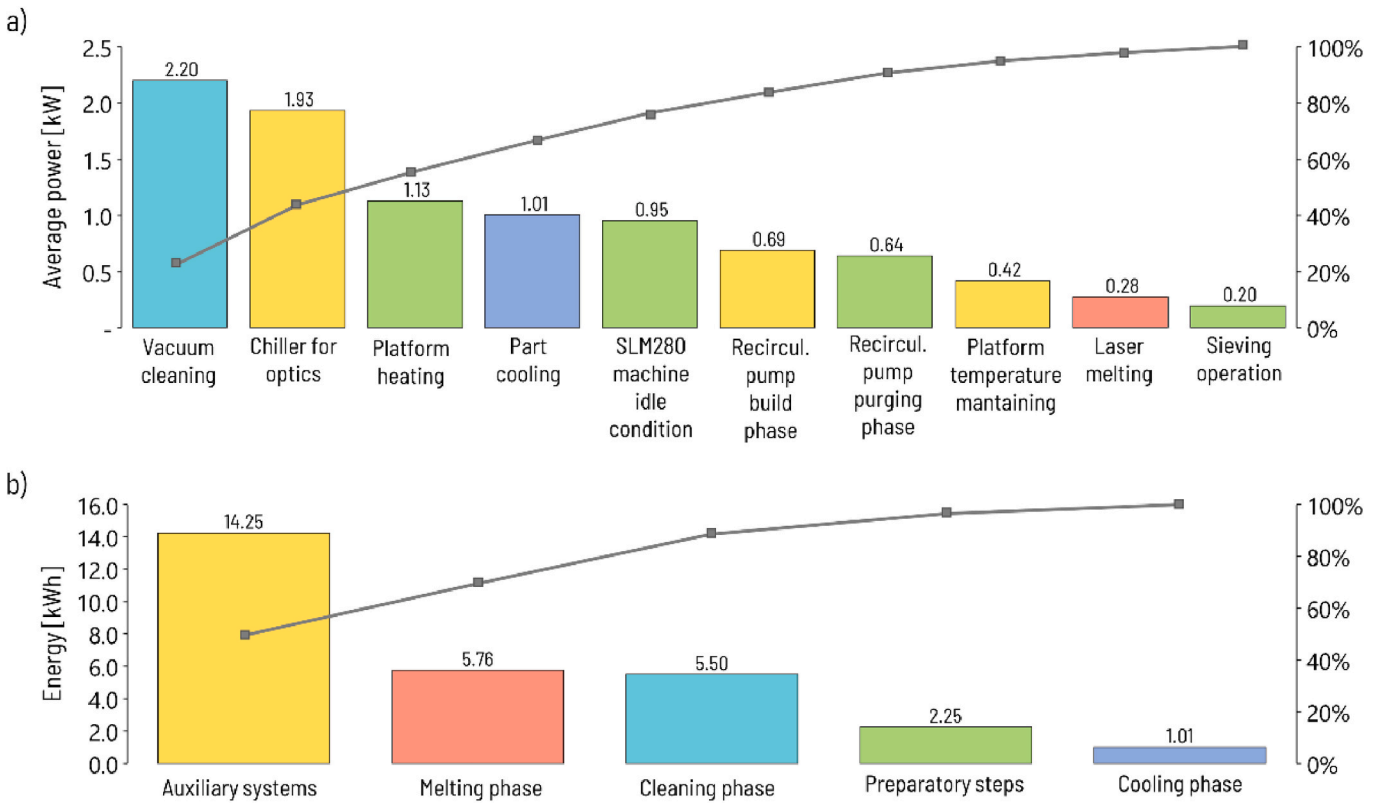

Fig. 5. Pareto analysis of: a) the average power consumption of the sub-systems; and b) the energy consumption of the unit activities; in a PBF-LB/M job.

required for each unit activity. The results show that the power consumption of few subsystems - in particular vacuum cleaning, cooling of the optics and platform preheating - dominates the power consumption and accounts for around 50% of the total power consumption. In terms of energy requirements for a typical job, the auxiliary systems alone are responsible for almost half of the total energy and therefore contribute significantly to the overall environmental impact of electricity consumption in the process.

Regarding the other two input resources involved in the process, which are listed in Table 4, the amount of metal powder required is estimated taking into account two key factors. The first is the powder volume required to complete the build, calculated from the product of the platform area, the z-height of the part, and the apparent density of the AlSi10Mg powder. Considering cubic geometries with a z-height of 48 mm, the total input mass of aluminum powder required per build is estimated at 6.47 kg for each of the four samples. The second accounts the experimentally measured overflow powder that accumulates in the side tank during each recoating cycle. A powder recycling rate of 96% is applied, reflecting standard industrial practices. Argon consumption is divided into two components: a fixed quantity of 1.18 kg used for initial chamber purging, resulting from a consistent flow rate applied for a limited amount of time in the pre-processing phase, and a variable portion linked to the active build phase, estimated from the average flow rate maintained throughout the manufacturing process.

Table 4
Overall argon and metal powder consumption for the gyroid samples.

	AlSi10Mg powder	Argon	
Part ID	Net powder consumption [kg]	Construction phase [kg]	Overall consumption [kg]
G-size 4	0.35	2.5	3.7
G-size 6	0.33	2.2	3.4
G-size 8	0.31	2.0	3.2
G-size 12	0.29	1.8	3.0

Building on this dataset, a more comprehensive evaluation of raw metal powder consumption was carried out using the Material Flow Analysis (MFA) approach, which mirrors the earlier assessment of electrical energy consumption and provides critical insights into resource efficiency. MFA examines both the input and output flows of materials throughout the manufacturing process, enabling the calculation of Material Utilisation Efficiency (MUE), defined as the ratio between the material effectively used to produce the final product and the total material consumed, taking into account both the material used in production and the waste generated. The formal definition of MUE within manufacturing sustainability studies is provided by Reich-Weiser et al. (2013), who describe material flow analysis as a key metric for green manufacturing, supporting the identification and quantification of material stocks and flows, including in complex production systems. The recycling ratio of 96% mentioned above assesses the environmental footprint of the resource in relation to the initial volume of material, which far exceeds the mass of the final consolidated part, thus providing the possibility of recycling and reusing this quantity directly reintroduced into the system. In contrast, the MFA approach measures the MUE by comparing the mass of the final part with the waste produced, which in this study consists mainly of the powder lost during the cleaning process and captured by the filtration system, totalling 0.26 kg. In general, the mass of support structures would contribute to the waste, but this is not true for the particular self-supporting samples analysed in this study. This analysis reveals that, in this specific case, the process has a low efficiency, with MUE rates of 27%, 21%, 17% and 11% for cell sizes from 4 mm to 12 mm. It is important to mention a limitation of this result: Since the calculations assume the production of only one sample per job, the MUE is greatly underestimated compared to standard industry practise. Launching a job where the build platform is largely

empty, i.e. the build volume is under-utilised, will result in a much greater flow of powder into the system than used for the actual construction, and therefore much higher losses than typical. Although this limits the meaningfulness of the absolute values for MUE on a more general level, the variation of this indicator with different cell sizes is reliable and still emphasizes a distinctive aspect of the PBF-LB/M process, namely that the scrap ratio increases with increasing inefficiency of nesting parts in the build volume The decreasing efficiency is due to the fact that the reduction in consolidated mass with larger geometries is not matched by a corresponding reduction in powder waste, which remains relatively constant due to the process characteristics, highlighting the need for new strategies to minimise material waste and improve resource efficiency, especially for lightweight geometries.

3.2. Environmental impact assessment

This data on primary resource consumption for the process is then used as input for measuring the environmental impact through a cradle-to-gate LCA. A first numerical result is fully described in Table 5 and graphically reported in Fig. 6, which show the midpoint comparative analysis of the gyroid structure with the four evaluated elementary cells.

This initial analysis confirms the previously observed trend: a reduction in unit cell size leads to an increase in the environmental impact of the manufacturing process. This result is driven by the extended manufacturing time associated with smaller unit cells, which consequently increases the consumption of all associated primary resources. Specifically, the sample with a cell size of 4 mm, which has the longest build time, also exhibits the highest environmental impact among the geometries evaluated.

In addition, a detailed analysis of the environmental impact from the midpoint assessment shows that electricity consumption during the PBF-LB/M process has the highest environmental burden among all resources assessed. The largest contribution to the stratospheric ozone depletion category is the emission of 1.53 E−05 kg CFC-11 eq. of nitrous oxide in air, from sludge incineration, which is related to the energy used to operate auxiliary equipment and the laser. Nitrogen oxide emissions to air from coal-based electricity generation drive ozone formation affecting human health and ecosystems. Sulphur dioxide emissions contribute significantly to the formation of fine particulate matter and soil acidification. Electricity generation from natural gas also has an impact on the mineral and fossil resource depletion categories. Water consumption, which amounts to 0.58 m^3, is largely due to the Italian electricity mix, particularly hydroelectric power, which partially mitigates its impact by contributing to water recovery. In addition to the impact of electricity consumption, gas atomisation for AlSi10Mg powder significantly affects ionizing radiation due to 4.7 kBq Co-60 eq Radon-222 emissions linked to uranium tailings treatment. Despite a high recycling rate of raw materials, processes such as the use of argon and electricity consumption still play an important role in the overall environmental footprint. Copper emissions from scrap treatment affect freshwater and marine ecosystems, while iron ore use drives mineral and fossil resource depletion. Argon consumption during the printing phase has a strong impact on freshwater eutrophication, with 71.8% of this effect attributable to phosphate emissions. Transport, SLM machine production, and aluminium recycling also contribute modestly to terrestrial ecotoxicity and human toxicity categories.

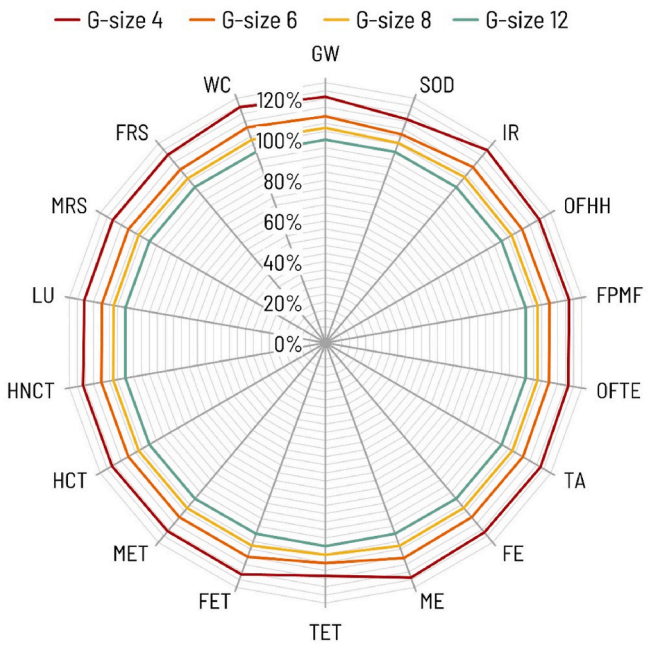

Fig. 6. Midpoint environmental impacts of the four cubic samples (ReCiPe, 2016; H method).

Global warming (GW) is a critical indicator for assessing the environmental impact of a process, primarily because of the global effort to reduce greenhouse gas emissions and secondarily because of its simplicity and effectiveness in measuring impact, so it is widely used both in environmental assessments and in corporate decision-making, as highlighted by Shine (2009) and Shine et al. (2005). The results show a carbon footprint (CFP) of 19.6, 20.8, 21.9 and 23.8 kg CO_2eq. for cell sizes of 12 mm, 8 mm, 6 mm and 4 mm, respectively. These values highlight a progressive increase in emissions as the cell size decreases,

Table 5
Midpoint environmental impacts (ReCiPe, 2016; H) of the four cubic samples, all manufactured with PBF-LB/M technology with AlSi10Mg alloy.

Impact category	Unit	G-size 4	G-size 6	G-size 8	G-size 12
Global warming	kg CO2 eq	2.38E+01	2.19E+01	2.08E+01	1.96E+01
Stratospheric ozone depletion	kg CFC11 eq	1.93E-05	1.80E-05	1.72E-05	1.65E-05
Ionizing radiation	kBq Co-60 eq	4.91E+00	4.48E+00	4.22E+00	3.97E+00
Ozone formation, Human health	kg NOx eq	4.51E-02	4.15E-02	3.94E-02	3.72E-02
Fine particulate matter formation	kg PM2.5 eq	3.19E-02	2.93E-02	2.78E-02	2.62E-02
Ozone formation, Terrestrial ecosystems	kg NOx eq	4.63E-02	4.26E-02	4.04E-02	3.81E-02
Terrestrial acidification	kg SO2 eq	8.33E-02	7.64E-02	7.23E-02	6.82E-02
Freshwater eutrophication	kg P eq	1.25E-02	1.15E-02	1.09E-02	1.03E-02
Marine eutrophication	kg N eq	1.11E-03	1.02E-03	9.60E-04	9.03E-04
Terrestrial ecotoxicity	kg 1,4-DCB	1.02E+02	9.63E+01	9.27E+01	8.89E+01
Freshwater ecotoxicity	kg 1,4-DCB	1.67E+00	1.54E+00	1.46E+00	1.37E+00
Marine ecotoxicity	kg 1,4-DCB	2.22E+00	2.05E+00	1.95E+00	1.84E+00
Human carcinogenic toxicity	kg 1,4-DCB	2.63E+00	2.43E+00	2.30E+00	2.17E+00
Human non-carcinogenic toxicity	kg 1,4-DCB	3.76E+01	3.47E+01	3.29E+01	3.10E+01
Land use	m2a crop eq	1.56E+00	1.44E+00	1.37E+00	1.29E+00
Mineral resource scarcity	kg Cu eq	1.34E-01	1.24E-01	1.18E-01	1.11E-01
Fossil resource scarcity	kg oil eq	7.08E+00	6.53E+00	6.20E+00	5.87E+00
Water consumption	m^3	7.24E-01	6.62E-01	6.24E-01	5.87E-01

by 6%, 11% and 21% for the 8 mm to 4 mm cells respectively, compared to the largest unit cell. This result emphasizes the significant role that cell size optimisation can play in reducing the carbon footprint of AM processes. A more detailed analysis of the most impactful sample (G-size 4) reveals that the production of a final part of only 0.093 kg leads to the emission of 23.8 kg CO_2eq., which is due to the combination of different factors in the PBF-LB/M. As illustrated in Fig. 7, electricity use accounts for 50% of the impact, followed by argon production (21%) and metal powder consumption (15%), despite partial powder recycling. Notably, 90% of GW potential stems from fossil fuel emissions, especially coal-based electricity. This points out the pivotal role that energy consumption and its source mix play in determining the environmental footprint of PBF-LB/M technology.

The overall environmental impact of each design is quantified also using a single index, known as eco-indicator points (Pt). This metric results from normalizing and weighting all relevant impact categories, with specific mathematical procedures varying by assessment method. As shown in Fig. 8 and detailed in Table 6, the Pt scores for samples with cell sizes of from 4 to 12 mm are 1.061, 0.977, 0.926, and 0.874 respectively. These values mirror the trends observed in the GW impact category. This correspondence is not coincidental: 95.5% of the total damage is attributed to the "Human Health" damage category, and within this category, global warming and fine particulate matter formation contribute the most to human health. These are primarily due to CO_2 emissions from fossil sources associated with the production of the resources used in the process.

4. Experimental validation

To validate the resource and impact assessment experimentally, one of the four cubic samples is produced. The sample is used to assess the manufacturability of the complex geometries under investigation and to check whether the actual resource consumption differs from the original estimates. The sample chosen for validation, G-size 12 is selected because it has consistently served as a reference in previous evaluations. The cube is produced according to the manufacturing setup described in section 2.1 to ensure the production of a single part and the measurement of its production time, avoiding possible interference from additional geometries. After the construction, the final dimensions of the part are assessed using a well-established methodology tailored to the evaluation of dimensional accuracy, taking into account the specific characteristics of the process. The mass is measured using an Ohaus PA124C analytical balance (Ohaus Europe GmbH, Switzerland). This is followed by a detailed inspection under a calibrated Nikon SMZ1270 stereomicroscope (Nikon, Japan), focusing on three views characteristic of the relevant orientations in the PBF-LB/M machine (the front, side, and top views), following the inspection protocol applied and described by Bassoli et al. (2023) in their study on dimensional accuracy and surface characterization of additively manufactured lattice structures. The environmental impact of the sample is then reassessed by collecting empirical data on the build time and final mass, which enables a recalculation of the resource consumption and overall environmental footprint.

The sample is produced successfully and in acceptable quality, demonstrating that even complex geometries can be manufactured effectively even with a printing strategy that was not optimised for thin-walled structures.

However, there are considerable deviations from the nominal geometry. Fig. 9 shows an example of the calibrated images used for the dimensional measurements. The dimensional evaluation shows some discrepancies in wall thickness between the nominal geometry and the actual manufactured part, especially in the measurements taken in the front and side views, where the walls are thicker than designed, probably due to the downskin and overhang effects. Dimensions parallel to the XY plane measured in the top view show a better accuracy of horizontal features. Nevertheless, the results are in line with the results of the feasibility study by Defanti et al. (2024). An increase of 15% in the manufactured mass of the part compared to the nominal value is found, which is consistent with the observed variations in wall thickness, but still within acceptable limits for the purpose of the study. The discrepancy between the estimated and actual build time is more marked and needs to be discussed. The recorded experimental build time is 4 h and 14 min, 28% longer than the estimated time of 3 h and 19 min. This difference can be attributed to software limitations in estimating the build time, especially in the case of non-optimised scan vectors of the laser. As these determine the path of the laser and the movement of critical components such as mirrors and optics, inefficient strategies, for instance with consecutive short paths like in the saddle region of this case study, can lead to increasingly longer times for repositioning the laser, ultimately increasing the overall production time. This increase in experimental build time contributes proportionally to higher environmental burden, primarily due to increased use of time-dependent inputs such as electrical energy and inert gas. In contrast, the contribution of metal powder remains relatively unchanged, as the slight variation in part mass across samples has a negligible effect on the total material-related impact. The longer build time can therefore be quantified in the GW impact category, and the revised LCA of sample G-size 12 results in 22.0 kg CO_2-equivalent emissions, 12% more than the original estimate. Considering the experimental results for the selected sample and the observed differences between the estimated and experimental data, it is reasonable to expect similar deviations for all other cubic samples with the same percentage. The recalculated global warming impact values reflecting this 12% increase are shown in Fig. 10. The experimental validation of build time estimates using a single sample represents a limitation of this study. Although this approach reflects established corporate practice and enables consistent comparison between estimated and measured data, the robustness of time-dependent resource assessment would be improved by a larger experimental dataset. Additionally, the analysis is based on a specific set of PBF-LB/M process parameters optimised for AlSi10Mg thin-walled structures. While this ensures internal consistency, different scan strategies, parameter sets, or materials may result in variations in build time, energy consumption, and environmental impact. Therefore, the conclusions of this work should be interpreted within the investigated manufacturing conditions. Future studies involving multiple samples and alternative process set-ups would further strengthen the universality of the proposed methodology and extend its applicability to other materials and lattice configurations.

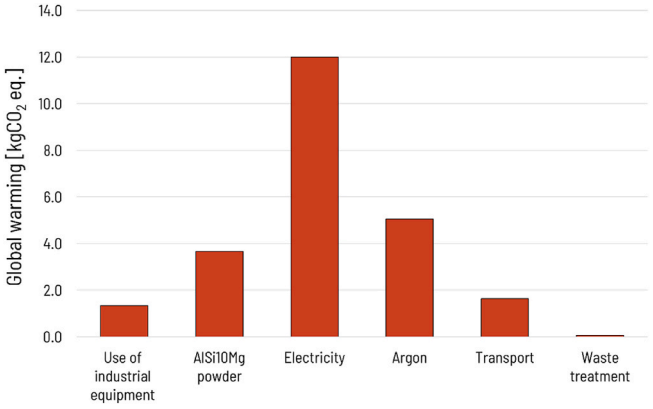

Fig. 7. Global warming impact related to the manufacture of the G-size 4 sample of 0.093 kg, detailed on all characteristic elements of PBF-LB/M.

5. Performance map and further research direction

The results described in the previous sections are used for an overall assessment of the comparison of the lattice structures investigated in this

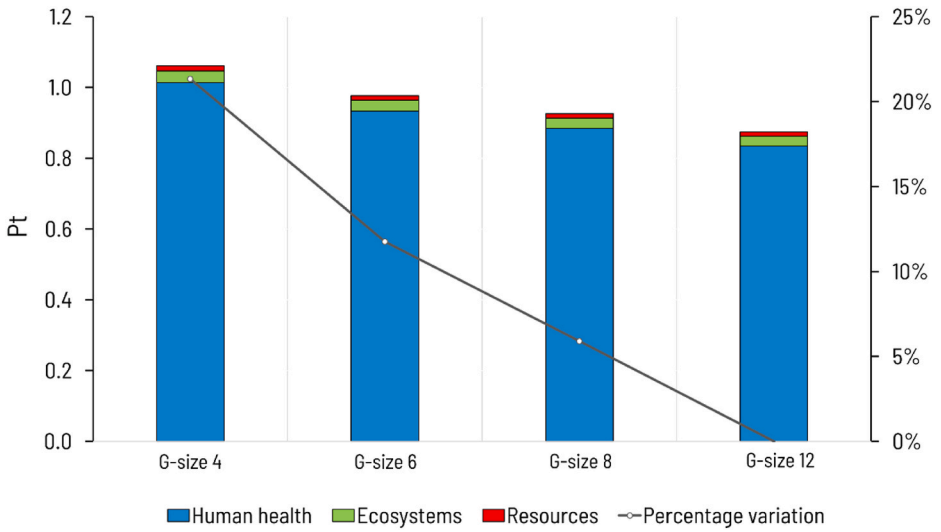

Fig. 8. Single score evaluation for the case study, obtained as the sum of the three scores given to the protection areas characterising the method.

Table 6
Endpoint assessment for the four gyroid samples.

Damage category	Unit	G-size 4	G-size 6	G-size 8	G-size 12
Human health	Pt	1.014	0.933	0.885	0.835
Ecosystems	Pt	0.033	0.030	0.029	0.027
Resources	Pt	0.015	0.014	0.013	0.012
Total	Pt	1.061	0.977	0.926	0.874

study, particularly with regard to how productivity and environmental impact vary with different cell sizes. When choosing a particular lattice structure for the design of a component, the designer must now consider and weigh up many different aspects and include the impact on the environment in the design specifications. By combining these assessments with traditional engineering key performance indicators, such as mass and structural properties, a robust framework for evaluating the overall performance of these structures can be developed, facilitating the selection of optimal designs tailored to specific application requirements and enabling the integration of novel parameters into performance mapping. The proposed evaluation approach can be formulated using newly defined coefficients for comparing different properties or using visual diagrams to easily assess the evolving properties as a function of the different unit cell size.

A first application of this approach is proposed in Table 7, where the results of this study for productivity and carbon footprint are combined with the structural properties measured by Defanti et al. (2024). The study deals with the compressive behaviour of the same lattice structures investigated here, except for the gyroid structure with a 4 mm unit cell. From the experimentally validated CFP values (CFP_{val}), metrics are calculated in Table 7 that can describe how the environmental impact is combined with other characteristics. In particular, the CFP per unit mass is given in column 4. In this study, a functional unit of a fixed volume was chosen to compare identical volumes filled with gyroid structures of

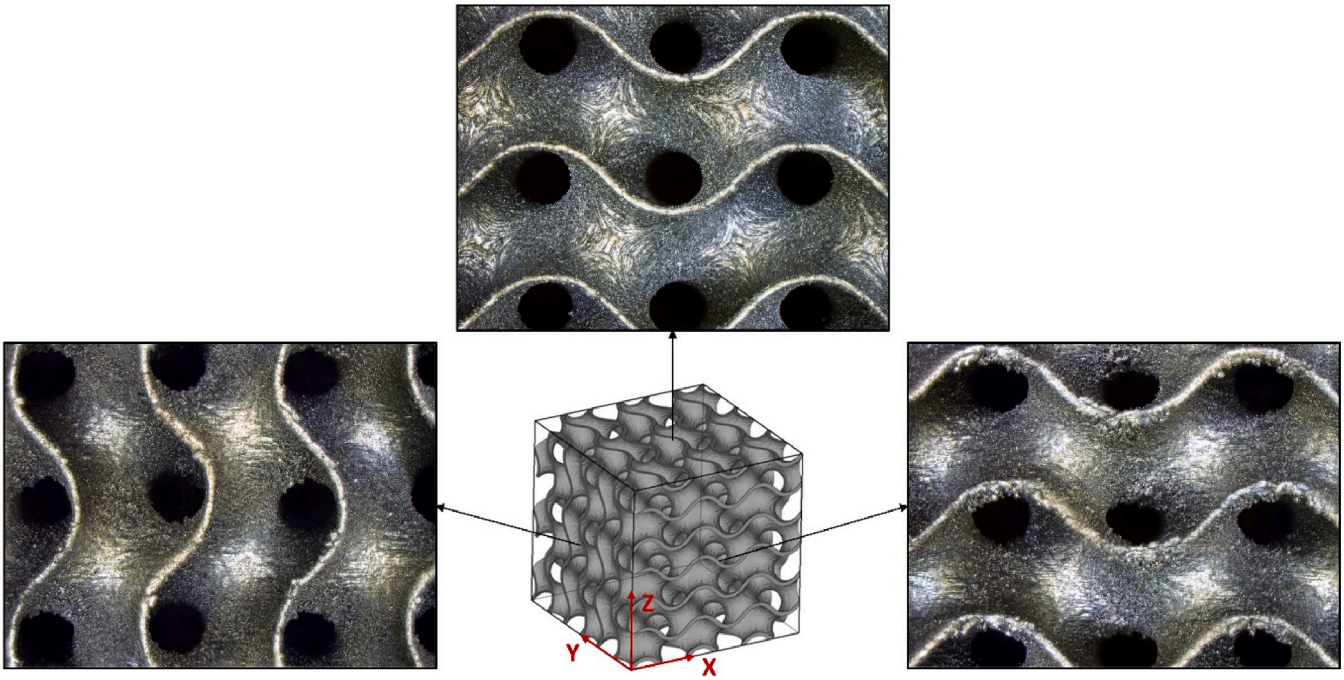

Fig. 9. Views of the dimensional measurements of the gyroid G-size 12 sample.

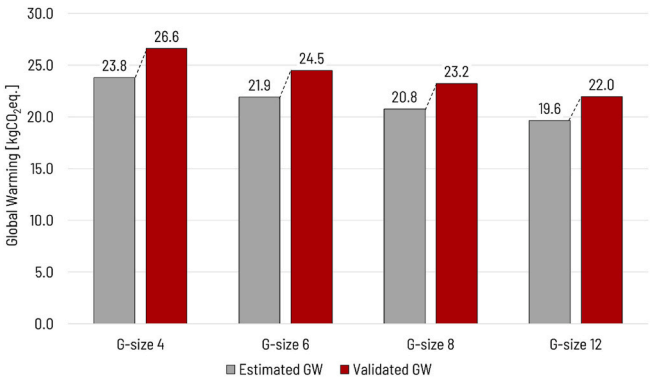

Fig. 10. Reassessed GW impact category reflecting the 12% increase between experimental and estimated values.

different cell size and thus different mass. This choice arises from the fact that lattice structures are often used by the designer to reinterpret the results of topological optimisation or, in any case, to model areas of the component where an intermediate density between that of solid material and hollow zone is required, i.e. they are used as metamaterials whose density and mechanical properties can be modulated according to the size of the cell. The result is that the CFP reported in column 2 shows a decreasing impact from the 4 mm cell to the 12 mm cell. If the reverse concept is applied, i.e. assuming equivalence of mass distributed over gyroid structures of different geometry (and volume), then the comparison is reversed as in column 4. In terms of impact per unit mass, the 12 mm cell gives a CFP that is more than twice that of the 4 mm cell. In line with the described approach, Table 7 proposes the development of new coefficients to enable comprehensive assessments, specifically the values of CFP per unit of compressive strength and per unit of modulus of elasticity. The evaluation of these coefficients shows that the adoption of lattice structures with smaller cell sizes leads to a higher specific compressive strength or stiffness, coupled with a reduction in CFP per unit structural feature. The result is that for structural applications designed for strength or stiffness, the adoption of smaller unit cells allows the environmental impact to be limited, i.e. a greener design for structural performance. These considerations allow to reflect on the importance of using appropriate metrics in additive manufacturing to obtain reliable results. While this study is limited to a cradle-to-gate approach, expanding the assessment to include the use phase could highlight the environmental savings related to mass reduction for automotive applications and offer a more holistic perspective.

Fig. 11 provides a graphical representation of the results. The performance of each cubic sample, with respect to the selected KPIs, is shown with normalized values ranging from 0% to 100% (at the extremes of the diagram). The map provides a straightforward qualitative visualization of the structures' performance as the unit cell size varies. By integrating data from multiple studies with different perspectives, such graphs can be further populated to create a robust tool for decision making.

A critical analysis of the results for this case study highlights that defining the environmental impact of the investigated AM process remains challenging. A key reason is the lack of standardised parameters that accurately capture both the environmental burden and the unique features of AM technologies. For example, the commonly used carbon footprint metric, expressed as $kgCO_2$ equivalent per unit mass, does not fully account for the benefits of complex geometries, which cannot be adequately represented by mass-based metrics alone. Furthermore, current approaches to assessing raw material consumption in AM are inconsistent, lacking detailed evaluation of the ratio of discarded material to final part mass and the proportion of recycled powder. These findings indicate the need for new AM-specific metrics, which could be integrated into standards and provide a systematic framework for combining data from different materials, AM methods, and application contexts.

Assessing the environmental impact of the process provides both a snapshot of its current sustainability status and a starting point for designing mitigation strategies. A significant portion of global warming impact originates from electricity generation, especially when fossil-based, which can be reduced through certified renewable energy sources. Additional measures, such as optimising process-related factors and expanding the system boundary to include the environmental benefits of weight reduction during the use phase, can further reduce the overall burden. Colombini et al. (2025) quantify that substantial improvements in cleaner and more sustainable AM can be achieved by simultaneously enhancing machine energy efficiency, increasing the use of secondary aluminium powders, and adopting lower-impact shielding gases. Implementing these strategies individually provides limited gains, whereas their combined application produces a substantial cumulative reduction in environmental impact. While these interventions fall beyond the direct scope of the present study, which focuses on design-driven effects, their integration with geometry optimisation represents a promising pathway towards cleaner and more sustainable additive manufacturing.

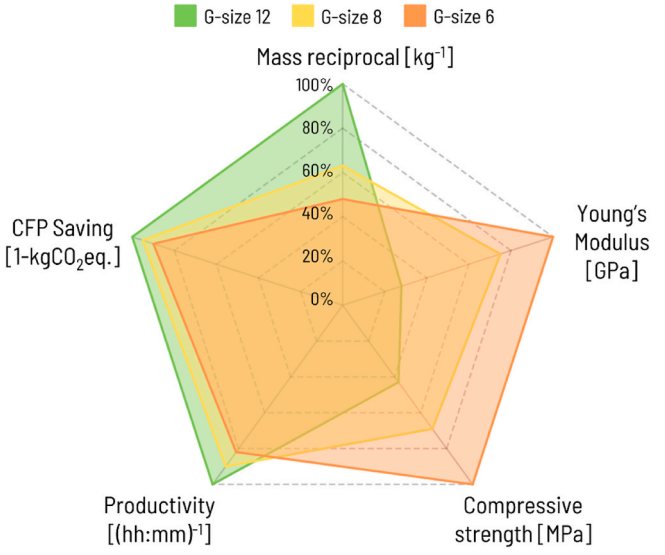

Fig. 11. Performance diagram of the gyroid structures with different cell size.

Table 7
Comparison of the validated environmental impact (CFP_{val}) and the structural properties of compressive strength (σ_r) and Young's modulus (E) obtained by Defanti et al., as the elementary cell varies.

Part ID	CFP_{val} [$kgCO_2eq.$]	Validated mass [kg]	CFP_{val}/kg [$kgCO_2eq./kg$]	σ_r [MPa]	CFP_{val}/ σ_r [$kgCO_2eq./MPa$]	E [GPa]	CFP_{val}/E [$kgCO_2eq./GPa$]
G-size 4	26.60	0.11	241.82	-	-	-	-
G-size 6	24.48	0.08	306.00	30.70	0.80	3.60	6.80
G-size 8	23.21	0.06	386.83	21.30	1.09	2.70	8.60
G-size 12	21.95	0.04	548.75	13.10	1.68	1.00	21.95

6. Conclusions

Based on a critical analysis of current environmental assessment methods for additive manufacturing technologies and with the aim of proposing tailored methodologies, this study illustrates a combined assessment of the environmental impact and productivity of manufacturing TPMS gyroid structures using PBF-LB/M process. Starting from a comparative cradle-to-gate LCA of cubic samples with cell sizes of 4, 6, 8 and 12 mm, the study critically discusses the metrics currently used for the evaluation of AM processes and proposes the introduction of new key performance indicators for mapping the performance of these structures.

The main concluding considerations of this study are as follows.

- The environmental impact of the PBF-LB/M process is largely dominated by auxiliary systems and shielding gas, making the carbon footprint (CFP) primarily a function of build time. In the considered case study, smaller unit cell sizes lead to longer build times and higher resource consumption, resulting in increased CFP within the global warming category.
- CFP increases at a slower rate than mass, compressive strength, or stiffness as cell size decreases, highlighting the complexity of selecting an optimal unit cell dimension that balances mechanical performance, lightweight design, and sustainability.
- A balance between structural, lightweight, and sustainability drivers can be sought by developing refined metrics specific to AM that accurately capture the unique characteristics of these processes.
- By combining traditional engineering metrics with these newly defined coefficients and visual performance maps, this study proposes a robust framework for evaluating overall part performance, supporting more informed and sustainable design choices.

CRediT authorship contribution statement

Giulia Colombini: Writing – review & editing, Writing – original draft, Methodology, Investigation, Data curation, Conceptualization. **Silvio Defanti:** Methodology, Investigation, Formal analysis, Conceptualization. **Federico Torri:** Methodology, Investigation, Data curation. **Elena Bassoli:** Writing – review & editing, Writing – original draft, Supervision, Methodology, Investigation, Conceptualization.

Declaration of competing interest

The authors declare that they have no known competing financial interests or personal relationships that could have appeared to influence the work reported in this paper.

Acknowledgements

The authors acknowledge HPE GROUP for their contribution during the experimental phase of this research. They also acknowledge the University of Modena and Reggio Emilia for supporting the activity by the "Fondo di Ateneo per la Ricerca 2022 per il finanziamento di piani di sviluppo dipartimentale nell'ambito della ricerca" (FARD 2022) and the "Fondo di Ateneo per la Ricerca 2022 - Bando per il finanziamento di progetti di ricerca interdisciplinari Mission Oriented – Linea FOMO" (FAR2022) and also the financial support of the European Union, NextGenerationEU - in the framework of the National Sustainable Mobility Center - MOST, CN00000023, Italian Ministry of University and Research Decree n. 1033— June 17, 2022, Spoke 12.

Data availability

Data will be made available on request.

References

ASTM International, 2022. ASTM E2986 – 22 - Standard Guide for Evaluation of Environmental Aspects of Sustainability of Manufacturing Processes.
ASTM International, 2022. ASTM E3012 – 22 - Standard Guide for Characterizing Environmental Aspects of Manufacturing Processes.
Azman, A.H., Vignat, F., Villeneuve, F., 2018. Cad tools and file format performance evaluation in designing lattice structures for additive manufacturing. J Teknol 80. https://doi.org/10.11113/jt.v80.12058.
Bassoli, E., Mantovani, S., Giacalone, M., Merulla, A., Defanti, S., 2023. On the technological feasibility of additively manufactured self-supporting AlSi10Mg lattice structures. Adv. Eng. Mater. 25. https://doi.org/10.1002/adem.202201074.
Campo, G.A., Vettorello, A., Giacalone, M., 2019. Optimization methodology for continuous heterogeneous structures: a preliminary design of an engine mounting bracket. Key Eng. Mater. 827, 116–121. https://doi.org/10.4028/www.scientific.net/KEM.827.11.
Colombini, G., Giacalone, M., Torri, F., Berni, F., Mantovani, S., Defanti, S., Bassoli, E., 2025. Effect of cell size on the environmental impact of gyroid lattice structures. Proced. CIRP 135, 161–166. https://doi.org/10.1016/j.procir.2024.12.013.
Colombini, G., Rosa, R., Ferrari, A.M., Defanti, S., Bassoli, E., 2024. Life cycle assessment of lattice structures: balancing mass saving and productivity. J. Clean. Prod. 445, 141390. https://doi.org/10.1016/j.jclepro.2024.141390.
Defanti, S., Giacalone, M., Mantovani, S., Tognoli, E., 2024. Dimensional and mechanical assessment of gyroid lattices produced in aluminum by laser powder bed fusion. Meccanica. https://doi.org/10.1007/s11012-024-01854-7.
Feng, J., Fu, J., Yao, X., He, Y., 2022. Triply periodic minimal surface (TPMS) porous structures: from multi-scale design, precise additive manufacturing to multidisciplinary applications. Int. J. Extrem. Manuf. 4, 022001. https://doi.org/10.1088/2631-7990/ac5be6.
Huijbregts, M.A.J., Steinmann, Z.J.N., Elshout, P.M.F., Stam, G., Verones, F., Vieira, M., Zijp, M., Hollander, A., van Zelm, R., 2017. ReCiPe2016: a harmonised life cycle impact assessment method at midpoint and endpoint level. Int. J. Life Cycle Assess. 22, 138–147. https://doi.org/10.1007/s11367-016-1246-y.
International Organization for Standardization, 2006a. ISO 14040:2006 - Environmental Management - Life Cycle Assessment - Principles and Framework.
International Organization for Standardization, 2006b. ISO 14044:2006 - Environmental Management - Life Cycle Assessment - Requirements and Guidelines.
Mahmoud, D., Tandel, S.R.S., Yakout, M., Elbestawi, M., Mattiello, F., Paradiso, S., Ching, C., Zaher, M., Abdelnabi, M., 2023. Enhancement of heat exchanger performance using additive manufacturing of gyroid lattice structures. Int. J. Adv. Manuf. Technol. 126, 4021–4036. https://doi.org/10.1007/s00170-023-11362-9.
Mantovani, S., Campo, G., Giacalone, M., 2022. Steering column support topology optimization including lattice structure for metal additive manufacturing. Proc Inst Mech Eng C J Mech Eng Sci 236, 10645–10656. https://doi.org/10.1177/0954406220947121.
Ramirez-Cedillo, E., García-López, E., Ruiz-Huerta, L., Rodriguez, C.A., Siller, H.R., 2021. Reusable unit process life cycle inventory (UPLCI) for manufacturing: laser powder bed fusion (L-PBF). Prod. Eng. 15, 701–716. https://doi.org/10.1007/s11740-021-01050-6.
Reich-Weiser, C., Simon, R., Fleschutz, T., Yuan, C., Vijayaraghavan, A., Onsrud, H., 2013. Metrics for green manufacturing. In: Green Manufacturing. Springer, US, Boston, MA, pp. 49–81. https://doi.org/10.1007/978-1-4419-6016-0_3.
Samson, S., Tran, P., Marzocca, P., 2023. Design and modelling of porous gyroid heatsinks: influences of cell size, porosity and material variation. Appl. Therm. Eng. 235, 121296. https://doi.org/10.1016/j.applthermaleng.2023.121296.
Sciancalepore, C., Bondioli, F., Gatto, A., Defanti, S., Denti, L., Bassoli, E., 2017. DREAM: driving up reliability and efficiency of additive manufacturing. 2017 IEEE 3rd International Forum on Research and Technologies for Society and Industry (RTSI). IEEE, pp. 1–4. https://doi.org/10.1109/RTSI.2017.8065979.
Shine, K.P., 2009. The global warming potential—the need for an interdisciplinary retrial. Clim. Change 96, 467–472. https://doi.org/10.1007/s10584-009-9647-6.
Shine, K.P., Fuglestvedt, J.S., Hailemariam, K., Stuber, N., 2005. Alternatives to the global warming potential for comparing climate impacts of emissions of greenhouse gases. Clim. Change 68, 281–302. https://doi.org/10.1007/s10584-005-1146-9.
Sikandar, M. U., and Roozbeh Neshani "Next generation eco-materials revolution: CO2 emissions reduction via lattice-structured Additive Manufactured Lever Arms.".
Sola, A., Defanti, S., Mantovani, S., Merulla, A., Denti, L., 2020. Technological feasibility of lattice materials by laser-based powder bed fusion of A357.0. 3D Print. Addit. Manuf. 7, 1–7. https://doi.org/10.1089/3dp.2019.0119.
Su, J., Ng, W.L., An, J., Yeong, W.Y., Chua, C.K., Sing, S.L., 2024. Achieving sustainability by additive manufacturing: a state-of-the-art review and perspectives. Virtual Phys. Prototyp. 19 (1). https://doi.org/10.1080/17452759.2024.2438899.
Torri, F., Berni, F., Fontanesi, S., Mantovani, S., Giacalone, M., Defanti, S., Bassoli, E., Colombini, G., 2023. Evaluation of TPMS structures for the design of high performance heat exchangers. https://doi.org/10.4271/2023-24-0125.

Torri, F., Berni, F., Martoccia, L., Marini, A., Merulla, A., Giacalone, M., Colombini, G., 2025. Numerical comparison of TPMS structures for the design of an automotive engine oil cooler. https://doi.org/10.4271/2025-01-8155.

Verma, R., Kumar, J., Singh, N.K., Rai, S.K., Saxena, K.K., Xu, J., 2022. Design and analysis of biomedical scaffolds using TPMS-Based porous structures inspired from additive manufacturing. Coatings 12, 839. https://doi.org/10.3390/coatings12060839.

Yang, E., Leary, M., Lozanovski, B., Downing, D., Mazur, M., Sarker, A., Khorasani, A., Jones, A., Maconachie, T., Bateman, S., Easton, M., Qian, M., Choong, P., Brandt, M., 2019. Effect of geometry on the mechanical properties of Ti-6Al-4V Gyroid structures fabricated via SLM: a numerical study. Mater. Des. 184, 108165. https://doi.org/10.1016/j.matdes.2019.108165.